




TREAD: Token Routing for Efficient Architecture-agnostic Diffusion Training

Felix Krause, Timy Phan, Vincent Tao Hu, Björn Ommer
CompVis @ LMU Munich

Abstract

Diffusion models have emerged as the mainstream approach for visual generation. However, these models usually suffer from sample inefficiency and high training costs. This issue is particularly pronounced in the standard diffusion transformer architecture due to its quadratic complexity relative to input length. Recent works have addressed this by reducing the number of tokens processed in the model, often through masking. In contrast, this work aims to improve the training efficiency of the diffusion backbone by using predefined routes that store this information until it is reintroduced to deeper layers of the model, rather than discarding these tokens entirely. Further, we combine multiple routes and introduce an adapted auxiliary loss that accounts for all applied routes. Our method is not limited to the common transformer-based model - it can also be applied to state-space models. Unlike most current approaches, our method,  TREAD, achieves this without architectural modifications. Finally, we show that our method reduces the computational cost and simultaneously boosts model performance on the standard benchmark ImageNet-1K 256×256 in class-conditional synthesis. Both of these benefits multiply to a convergence speedup of $9.55\times$ at 400K training iterations compared to DiT and $25.39\times$ compared to the best benchmark performance of DiT at 7M training iterations. Our code will be released. Our code will be released at: <https://github.com/CompVis/tread>.

1. Introduction

In recent years, diffusion models [20, 41, 45] have become a powerful generative technique for image synthesis [22, 41]. They have also been successfully extended to the 3D [38] and video domains [3]. While diffusion models avoid some training challenges faced by their predecessors, such as GANs [14], they incur high costs [26] due to slow convergence and sample inefficiency [31]. Currently, the Diffusion Transformer (DiT) [35] is the main approach for scaling these models, building on the established Transformer architecture [53]. However, the Transformer architecture has computational

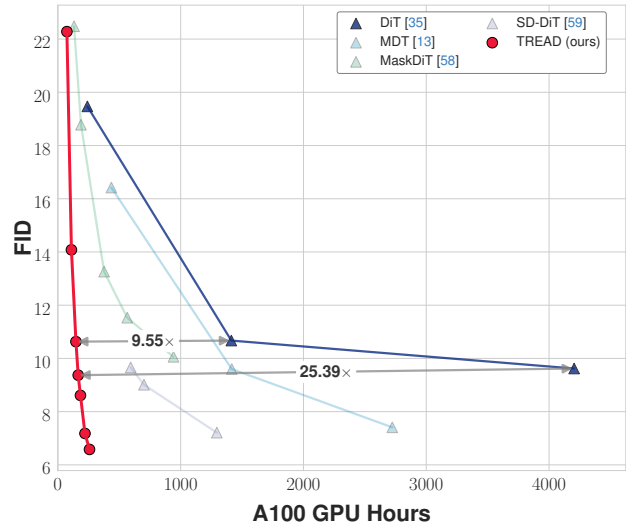


Figure 1. Our proposed diffusion training strategy, TREAD, offers better fidelity while retaining the computational efficiency of previous methods. We compare using FID as a measure for fidelity, and the required compute is presented using A100 hours. We show clear compute-efficiency improvements compared to DiT [35] and other existing methods that aim to reduce computational cost [13, 58, 59]. In our experimental setup, we outperform all presented methods, reaching a FID = 6.58 at only 256 A100 hours while MDT requires 2,724 A100 hours for comparable results and DiT reaches the best reported FID = 9.62 on ImageNet-1K 256×256 using 4,180 A100 hours.

cost limitations, as it scales quadratically with token length and converges slowly, further increasing the expense of training diffusion models. Training a DiT on standard benchmarks alone requires thousands of A100 GPU hours without reaching convergence, and text-to-image models demand even more—Stable Diffusion [41], for instance, required about 150,000 A100 GPU hours. Despite ongoing efforts to reduce computational demands through improved infrastructure, implementation, and hardware, democratizing the training of diffusion models remains a distant goal. Several works have proposed methods to accelerate the training convergence utilizing external self-supervised features [21, 55],

improved flow-based theory [27] or optimized data combinations [52, 57]. Another way to reduce computational resource requirements involves limiting the flow of information during training. This can be achieved by selecting information and directing it to specific computational blocks. Therefore, these tokens skip all computations along the way to reduce the overall workload. This is referred to as *routing* [40]. In addition to routing, the computational budget can be allocated to only a subset of the available information. This subset can be determined either by random chance [58] or through learned heuristics [32, 54], where the remaining information is disregarded indefinitely, a strategy known as *masking* [6, 17]. These methods have two possible advantages: (1) reducing compute requirements by processing fewer tokens [16, 58], and (2) enhancing convergence by encouraging contextual relation learning [2, 13], thereby addressing data efficiency and lowering computational demands. While masking has been extensively studied for both benefits and is a well-established technique in self-supervised and representation learning [2, 17], routing has primarily been considered from the standpoint of compute reduction alone [18, 40]. This work explores the routing technique for diffusion models using predefined routes that pass tokens from one layer deeper into the network. In contrast to masking, the loss of information is only temporary, as information will be reintroduced. We do this by defining a route with a start and end layer and a fixed ratio with which tokens are randomly selected. This is done only during training and without any dynamic adaptations based on iterations or timesteps. Extending this concept, we demonstrate the impact that multiple routes can have on the performance of a diffusion model and test the variance of different route configurations for robustness. Our main contributions can be summarized as follows:

- We investigate token-specific computational bypass techniques for diffusion models, providing insights into their underlying mechanisms. We introduce a training strategy based on these techniques that requires no architectural modifications while simultaneously improving both qualitative performance and training speed.
- Building on our initial exploration, we extend our approach from single-route to multi-route. Our framework enhances diffusion models across various architectures, demonstrating improvements in convergence speed for both the standard DiT and state space models.
- Most importantly, we not only match the performance of DiT with an FID of 19.47 but also improve upon it, achieving an FID of 10.63 under the same number of iterations and identical settings in the standard benchmark of class-conditional synthesis on ImageNet-1K 256×256. This results in a **9.55×** convergence speedup. Using the best FID of 9.62 reported by DiT-XL/2 as a baseline, we achieve a speedup of **25.39×** and reach a better FID of

9.32 within 41 hours.

2. Related Work

Diffusion Models and Efficient Generative Backbones

Score-based models [46, 47], such as Denoising Diffusion Probabilistic Models (DDPM) [20], have become the dominant framework for image synthesis in recent years. These models start with a Stochastic Differential Equation (SDE) and gradually add Gaussian noise to real data in the forward process. This process transforms the complex real distribution into a Gaussian distribution. An iterative denoising process is then used to reverse this transformation and generate samples. A key improvement in the efficiency of early diffusion models was moving the training to a compressed latent space [41].

Building on the foundation of score-based models, early diffusion models [7, 20, 41] used the UNet architecture [42] as their backbone. However, more recently, token-based models like DiT [35] have become a preferred backbone choice [5, 8, 58]. However, these models face challenges due to their quadratic complexity with respect to the number of tokens.

To address the computational challenges associated with token-based models, recent studies have proposed caching mechanisms to accelerate diffusion models based on UNets [29] or DiTs [30]. Unlike these approaches, our routing scheme does not skip the computation of network layers for each token. Instead, we introduce a routing mechanism that operates only during training. This mechanism transports tokens from one network layer to another, enhancing the model’s efficiency without omitting necessary computations.

In addition to diffusion transformers, state space models (SSMs) have recently been shown to be promising alternatives to DiTs [10, 12, 22, 51] to alleviate the quadratic complexity. However, largely owing to their recent rise, there are currently few works that push the efficiency of SSMs in a generative setting. Token pruning [56], token masking [50], and mixture-of-experts [37] for SSMs have been explored so far, although not for diffusion backbones. Different from them, we consider the token routing technique in state-space models to improve the training efficiency.

Token-based Routing, Pruning and Masking

Several recent methods [11, 34, 49] utilize the sparse Mixture-of-Experts (MoE) [23, 44] technique to improve the efficiency of diffusion transformers. Typically, MoE is implemented as a router module that divides the network into subsets, or experts. The router then determines which expert processes each token, thereby reducing computational overhead compared to applying every parameter to every token. Another strategy, Mixture-of-Depths (MoD) [40], involves a router module that decides the computation paths for each token

within the network, allowing tokens to skip certain computational blocks. MoD has been shown to decrease runtime costs while maintaining model performance in transformer-based language models. In contrast to these methods, our approach does not require a routing module. Instead, we introduce a training strategy that enhances efficiency without modifying the base architecture.

To further address the scalability issues associated with the attention mechanism, numerous studies [9, 32, 39, 54] have focused on pruning tokens based on their content, such as similarity or redundancy. This token pruning helps reduce the computational burden of the attention mechanism by eliminating less important tokens. While our approach also selects tokens to be disregarded, it differs from these prior works in that our routing scheme does not rely on the content of the tokens. Instead of pruning based on token characteristics, our method employs a routing mechanism that directs tokens through the network irrespective of their content, maintaining computational efficiency without sacrificing necessary computations.

In addition to pruning-based methods, recent advancements like MaskDiT [58] have proposed token masking schemes applicable to DiTs. MaskDiT improves convergence speed by significantly lowering the cost per iteration and accelerating training, all while matching the performance of standard DiTs. Building on this, SD-DiT [59] enhances generative quality by incorporating a discriminative loss alongside the masking strategy. Similar to these approaches, our scheme removes tokens at random. However, unlike MaskDiT, which replaces masked tokens with learnable embeddings, our method routes tokens back to later layers in the network.

3. Prerequisites

We adopt the framework established by Song et al. [48], which explores the forward diffusion and backward denoising processes of diffusion models in a continuous time context through the use of stochastic differential equations (SDEs). The forward diffusion process gradually transforms real data $\mathbf{x}_0 \sim p_{\text{data}}(\mathbf{x}_0)$ into a noise distribution $\mathbf{x}_T \sim \mathcal{N}(0, \sigma_{\text{max}}^2 \mathbf{I})$ with the following SDE:

$$d\mathbf{x} = \mathbf{f}(\mathbf{x}, t) dt + g(t) dW, \quad (1)$$

where \mathbf{f} represents the drift coefficient, g is the diffusion coefficient, W denotes a standard Wiener process, and the time variable t ranges from 0 to T .

In the reverse process, the generation of \mathbf{x}_0 samples is achieved through another SDE expressed as:

$$d\mathbf{x} = [\mathbf{f}(\mathbf{x}, t) - g(t)^2 \nabla_{\mathbf{x}} \log p_t(\mathbf{x})] dt + g(t) d\bar{W}, \quad (2)$$

where \bar{W} signifies a reverse-time Wiener process, and dt represents an infinitesimal negative timestep. This reverse

SDE can be reformulated into a probability flow ordinary differential equation (ODE), which retains the same marginal distributions $p_t(\mathbf{x})$ as the forward SDE at each timestep t :

$$d\mathbf{x} = \left[\mathbf{f}(\mathbf{x}, t) - \frac{1}{2} g(t)^2 \nabla_{\mathbf{x}} \log p_t(\mathbf{x}) \right] dt. \quad (3)$$

Utilizing the formulation of Karras et al. [24] (EDM), we simplify the drift term by setting $\mathbf{f}(\mathbf{x}, t) := 0$ and defining the diffusion coefficient as $g(t) := \sqrt{2t}$. Consequently, the forward SDE simplifies to the expression

$$\mathbf{x}_t = \mathbf{x}_0 + \mathbf{n}, \quad (4)$$

where $\mathbf{n} \sim \mathcal{N}(0, t^2 \mathbf{I})$. The corresponding probability flow ODE can be formulated with the score function $s(\mathbf{x}, t) := \nabla_{\mathbf{x}} \log p_t(\mathbf{x})$:

$$d\mathbf{x} = -t \mathbf{s}(\mathbf{x}, t) dt. \quad (5)$$

To estimate $s(\mathbf{x}_t, t)$, the EDM approach parameterizes a denoising function $D_{\theta}(\mathbf{x}_t, t)$ which minimizes the denoising score matching loss:

$$\mathbb{E}_{\mathbf{x}_0 \sim p_{\text{data}}} \mathbb{E}_{\mathbf{n} \sim \mathcal{N}(0, t^2 \mathbf{I})} \|D_{\theta}(\mathbf{x}_0 + \mathbf{n}, t) - \mathbf{x}_0\|^2, \quad (6)$$

where $\mathbf{x}_t = \mathbf{x}_0 + \mathbf{n}$, from this formulation, $s(\mathbf{x}_t, t)$ can be approximated as

$$\hat{s}(\mathbf{x}_t, t) = \frac{D_{\theta}(\mathbf{x}_t, t) - \mathbf{x}}{t^2}. \quad (7)$$

A common choice to formulate the denoising function $D_{\theta}(\cdot, \cdot)$ is the usage of a Diffusion Transformer or other scalable architectures like SSMS [22, 36]. We adopt the DiT due to its community-wide usage as our main model used for ablations shown in Section 5.

Masking-based Training Objective Using a standard training strategy for diffusion models, one can apply Equation (6) to the entire token set. However, if the diffusion model is trained only on a subset of tokens, either through masking, pruning or routing, the task becomes more challenging [58]. Specifically, the model must form predictions across the full set of tokens while only having access to a partial set. To address this, He et al. [17] propose to decompose the loss into two parts: 1) the denoising score matching loss and 2) the Masked AutoEncoder (MAE) loss. While the former one is applied only to the visible tokens, the MAE loss acts as auxiliary task for reconstructing masked tokens from visible ones. Zheng et al. [58] reason that the additional MAE loss can promote the model to develop a more global understanding of the full image.

For this, we first define the operators $\mathcal{V}_{\mathbf{m}}$ and its complement $\bar{\mathcal{V}}_{\mathbf{m}}$ to yield the partial token sets by applying a randomly sampled binary mask $\mathbf{m} \in \{0, 1\}^P$, where P

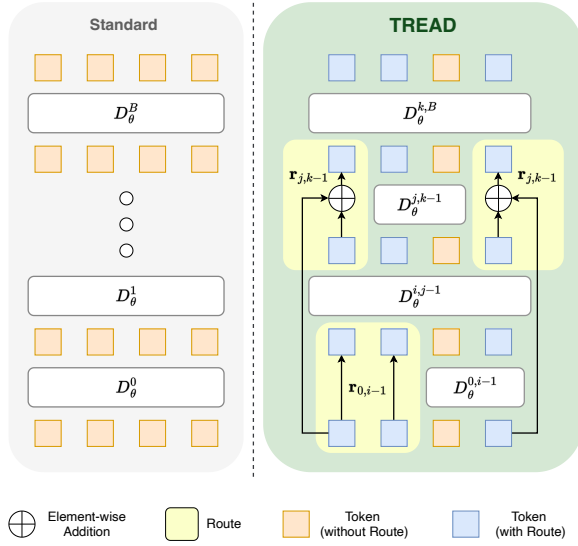


Figure 2. **TREAD: Our method for efficient diffusion training.** On the left, a simplified standard DiT architecture is shown consisting of B computational blocks. On the right, we show our training strategy, which does not affect the B computational blocks themselves. Instead, two routes $\mathbf{r}_{0,i-1}$ and $\mathbf{r}_{j,k-1}$ are shown that modulate the way these B blocks receive and process tokens. In this example, the blue tokens are affected by one or more routes while the orange tokens are affected by none, which is equivalent to the standard training strategy. All computational blocks contain the same structure and parameter number as their vanilla counterparts. Their respective width only corresponds to the number of processed tokens during training.

is the number of total patches. Therefore, we can define $\mathcal{V}_{\mathbf{m}}(\mathbf{x}) = (1 - \mathbf{m}) \odot \mathbf{x}$ and $\bar{\mathcal{V}}_{\mathbf{m}}(\mathbf{x}) = \mathbf{m} \odot \mathbf{x}$.

We then apply our denoising score matching loss (Equation (6)) to the token set $\bar{\mathcal{V}}$ which yields:

$$\mathcal{L}_{\text{dsm}} = \mathbb{E}_{\mathbf{x}_0 \sim p_{\text{data}}, \mathbf{n} \sim \mathcal{N}(0, t^2 \mathbf{I}), \mathbf{m}} \left\| \bar{\mathcal{V}}_{\mathbf{m}}(D_{\theta}(\mathbf{x}_0 + \mathbf{n}, t) - \mathbf{x}_0) \right\|^2, \quad (8)$$

where \odot is element-wise multiplication. We then formulate the second MAE loss solely on the token set in $\mathcal{V}_{\mathbf{m}}$. This leads us to:

$$\mathcal{L}_{\text{mae}} = \mathbb{E}_{\mathbf{x}_0 \sim p_{\text{data}}, \mathbf{n} \sim \mathcal{N}(0, t^2 \mathbf{I}), \mathbf{m}} \left\| \mathcal{V}_{\mathbf{m}}(D_{\theta}(\mathbf{x}_0 + \mathbf{n}, t) - \mathbf{x}_0) \right\|^2. \quad (9)$$

We combine those two terms with a weighting coefficient λ :

$$\mathcal{L} = \mathcal{L}_{\text{dsm}} + \lambda \mathcal{L}_{\text{mae}}. \quad (10)$$

4. TREAD

In this work, we introduce a broadly applicable diffusion training strategy using routes. These routes serve as a unidirectional mechanism to transport tokens across layers. Formally we define a route as:

$$\mathbf{r} = \{ (D_{\theta}^{l_i}, D_{\theta}^{l_j}) \mid 0 \leq i < j \leq B \}, \quad (11)$$

where:

- $B + 1$ is the total number of layers in the network D_{θ} ,
- $L = \{D_{\theta}^{l_1}, D_{\theta}^{l_2}, \dots, D_{\theta}^{l_B}\}$ is the set of layers in D_{θ} .
- Each pair $(D_{\theta}^{l_i}, D_{\theta}^{l_j}) \in \mathbf{r}$ represents a connection from the start layer $D_{\theta}^{l_i}$ to the end layer $D_{\theta}^{l_j}$.

For simplicity, we denote $\mathbf{r}(D_{\theta}^{l_i}, D_{\theta}^{l_j})$ as $\mathbf{r}_{i,j}$, where i is the starting layer and j is the ending layer. As illustrated in Figure 2, a selected route transports tokens from one layer to another. When the route $\mathbf{r}_{i,j}$ is active, the tokens are bypassed by all intermediate layers it spans. Once the route completes, these tokens become available again, allowing layer $D_{\theta}^{l_j}$ to receive information from layer $D_{\theta}^{l_i}$. We propose that the capability of Transformer-based models to interpret the output of preceding layers [18, 29, 30, 40] can be used during training to enhance the convergence speed of the noise-to-image mapping. This characteristic is also demonstrated using the cosine similarity between the produced outputs by each layer of a trained DiT in Figure 3. Although the exact underlying mechanisms are not yet fully theoretically grounded, our empirical results in Section 5 demonstrate the effectiveness of this token transportation method. We hypothesize that the semantic importance of the noise space [4, 43] plays a crucial role. By repeatedly supplying information about \mathbf{x}_t to the network, the learning of the noise-image mapping becomes more efficient. This is effectively achieved by using a route $\mathbf{r}_{0,j}$.

Additionally, each route $\mathbf{r}_{i,j}$ decreases the computational cost along its length, as tokens are not involved in any computation up to their reintroduction. However, similar to masking, there may exist a combination of *selection rate* of a given route $\mathbf{r}_{i,j}$ and the enhancements in convergence it enables.

Multi-Route \mathcal{R}^N for further acceleration. Intuitively, this principle promotes the exploration of consecutive routes, ensuring that more segments of the network can access the noise-space information more regularly. However, applying multiple routes, specifically $\mathbf{r}_{0,i}$ and $\mathbf{r}_{j,k}$, is more complex than using a single route. This complexity arises because when the first route $\mathbf{r}_{0,i}$ terminates, tokens are transferred from the input to layer $D_{\theta}^{l_{i+1}}$, filling the set of tokens back up to its original size. At this point, a new representation that spans the entire set of tokens is created. As a result, there are two primary objectives that need to be considered:

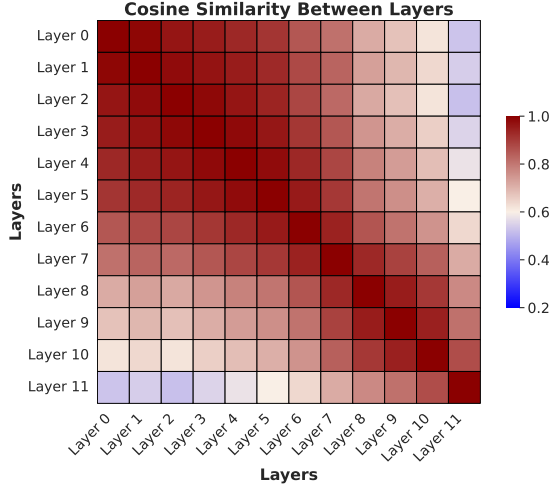


Figure 3. Neighbouring layers have highly similar output. Especially early layers share a particularly high similarity, while deeper layers (Layers 9, 10, 11) also show increased similarity. It is noteworthy that layers at opposing ends of the network still show a high similarity of around 0.5.

1. Introducing \mathbf{x}_t via route $\mathbf{r}_{j,k}$ to layer $D_\theta^{l_{k+1}}$,
2. Utilizing the already computed information from the layers between $\mathbf{r}_{0,i}$ and $\mathbf{r}_{j,k}$ to utilize the model's capacity efficiently.

To address these objectives without forcing a binary decision between them, we choose to use a linear combination of \mathbf{x}_t and the representation produced by the direct predecessor of $\mathbf{r}_{j,k}$, which is layer $D_\theta^{l_{j-1}}$. Specifically, this combination is defined as:

$$\gamma_{t,j-1} = \mathbf{x}_t + D_\theta^{l_{j-1}}(\cdot, \cdot) \quad (12)$$

This approach allows both objectives to be satisfied simultaneously by blending the new input with the existing representation from the preceding layer. The multi-route design is further illustrated in Figure 2, which provides a visual representation of how the routes interact within the network.

Multi-Route Ensemble Loss. In Section 3, we noted that withholding tokens increases task complexity. This added complexity can be managed by adjusting the loss functions, as defined in Equation (8) and Equation (9). The mask operator \mathbf{m} determines which tokens the loss function \mathcal{L}_{mae} applies to, with the mask corresponding to a specific route $\mathbf{r}_{i,j}$.

When we apply multiple routes \mathbf{r} , however, we must consider multiple masks \mathbf{m} to avoid ignoring the effect of withholding a significant amount of information. Existing literature and formulations typically handle only a single

mask operator \mathbf{m} , lacking the flexibility to support multiple masking scenarios.

To address this, we extend the formulation by introducing a set of routes \mathcal{R} . Here, \mathcal{R}^k denotes the k -th route in the set, where each route $\mathbf{r}^k \in \mathcal{R}^N$ includes its own binary mask. We define \mathcal{V}_m^k as an operator that selects tokens for the k -th route based on a random mask \mathbf{m} . We also introduce $\bar{\mathcal{V}}_m^k$, the complement operator.

With these definitions, we update the loss functions \mathcal{L}_{dsm} and \mathcal{L}_{mae} accordingly.

$$\mathcal{L}_{\text{dsm}}^k = \mathbb{E}_{\mathbf{x}_0 \sim p_{\text{data}}, \mathbf{n} \sim \mathcal{N}(0, t^2 \mathbf{I}), \mathbf{m}} \left\| \bar{\mathcal{V}}_m^k (D_\theta^{\mathcal{R}^k}(\mathbf{x}_0 + \mathbf{n}, t) - \mathbf{x}_0) \right\|^2, \quad (13)$$

and

$$\mathcal{L}_{\text{mae}}^k = \mathbb{E}_{\mathbf{x}_0 \sim p_{\text{data}}, \mathbf{n} \sim \mathcal{N}(0, t^2 \mathbf{I}), \mathbf{m}} \left\| \mathcal{V}_m^k (D_\theta^{\mathcal{R}^k}(\mathbf{x}_0 + \mathbf{n}, t) - \mathbf{x}_0) \right\|^2, \quad (14)$$

where $D_\theta^{\mathcal{R}^k}(\cdot, \cdot)$ represents the subnetwork of $D_\theta(\cdot, \cdot)$ defined by the k -th route in \mathcal{R} . Our final multi-route ensemble loss is formulated as \mathcal{L} :

$$\mathcal{L} = \frac{1}{N} \sum_{k=1}^N (\mathcal{L}_{\text{dsm}}^k + \lambda \mathcal{L}_{\text{mae}}^k), \quad (15)$$

where N denotes the total number of sequential routes employed.

5. Experiment

5.1. Experimental Details

Model Architecture. The overall structure of our model follows the two-stage training process of Latent Diffusion Models (LDM) [41] where we first train an autoencoder that translates back and forth between the pixel-level image space and its latent space. We use the pre-trained VAE from Stable Diffusion with the standard downsampling factor of 8. Even though the main requirement for our method is the usage of tokens, we choose a standard DiT [35] in the size XL and a patch size of 2 as our main model for ablation. Further, we also show the generalizability to other architectures like Diffusion-RWKV [12]. For ablations that do not require the largest model size, we either switch to model size B or S and use a patch size of 4, depending on the task. Any changes are clearly stated for each experiment. The application of our method is marked by the additional **-TREAD**. Additionally, the number of routes applied during training will be noted using **TREAD-1** for a single one while we use the respective increment for each additional route.

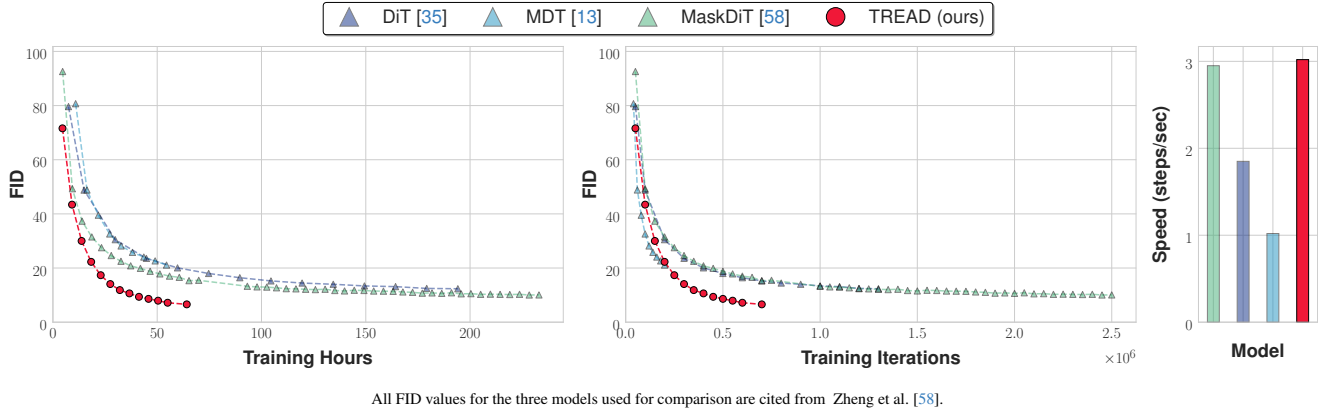


Figure 4. **TREAD outperforms the baseline DiT [35] and other compute-efficient methods [58].** We display FID versus Training Hours and FID versus Training Iterations to highlight TREAD’s faster convergence and fewer total iterations, amplified by a lower cost per iteration. While MDT-XL/2 achieves similar convergence in terms of iterations, its higher computational cost results in slower iteration speeds. MaskDiT performs comparably to DiT-XL/2 but is more efficient. TREAD strikes a balance between these methods, offering similar computational costs to MaskDiT with better per-iteration performance than MDT-XL/2. Values for DiT-XL/2, MDT-XL/2, and MaskDiT are cited from Zheng et al. [58]. Iterations per second were measured using an A100 GPU setup (batch size 64), corresponding to a batch size of 256 on four A100 GPUs, as used in our experiments.

Training Setup. We follow the standard of existing works on diffusion models and train models on ImageNet-1K 256×256 and a batch size of 256. Further, we follow the standard setting for the AdamW from the original DiT [35] with a learning rate of $1e-4$ and no weight decay and the standard β -parameters of 0.9 and 0.999 respectively. Except for experiments that specifically state otherwise, we apply a selection rate of 50% for each route. Further, we use an EMA model with an update rate of 0.9999. All results are computed using this EMA model. We do not employ any kind of data augmentation. All experiments are conducted on $4 \times 80\text{GB-A100 GPUs}$, resulting in a batch size of 64 per GPU. Therefore, the most impactful difference to the vanilla DiT in implementation is our adjusted loss formulation (Equation (15)). Further, we use precomputed latents of ImageNet-1K 256×256 , leading to a 32×32 representation. All of our runs are done with a mixed precision of `bf16` if not otherwise specified. Following Zheng et al. [58] we apply a weight λ of 0.1 on the MAE loss. For Transformer-based structures, we use random selection, while for sequential models like RWKV, we find that row selection works better.

Evaluation We utilize the Fréchet Inception Distance (FID) [19] as our main metric to evaluate the quality of our models and report the values on 50,000 samples if not otherwise specified as this is standard procedure for current ImageNet-based benchmarks [35, 55, 58]. We utilize ADM’s evaluation suite [7] to provide fair comparisons to prior works and baselines.

5.2. Main Result

Comparison with baseline architectures. We show the improvement using our proposed training strategy over DiT (see Table 1) and RWKV (see Table 2) with our method clearly improving upon the base architectures in any configurations. We compare our DiT S, B, and XL models to their respective counterparts while we present further comparisons to other efficiency-oriented methods using XL-sized models in Table 3. Notably, the improvements extend positively to larger models, leading to an FID of 12.47 with DiT-XL/2+TREAD-1. As discussed in Section 4, we also investigate the application of multiple routes. Using DiT-XL/2+TREAD-2 we are almost able to cut the FID in half (FID 19.47 \rightarrow 10.63) at 400K steps. Further, we also show DiT-B/2+TREAD-1 (random) as a baseline for randomly selecting the ending location of the route \mathbf{r} with a measured FID of 36.80. Its minimal difference to a predefined route (e.g. DiT-B/2+TREAD-1) indicates robustness against location configuration. This is explored in Table 6 in a more thorough manner. Lastly, Table 2 shows the extension of our method to SSMs with RWKV as a representative model. To adjust TREAD to RWKV, the used routes apply a row selection instead of random selectio which shows performance improvements (FID = 53.79) compared to our own Diffusion-RKVV baseline (FID = 59.84).

Comparison with Mask-based methods. First, we examine the speed measured in iterations per second using a single A100 with a batch size of 64 to indicate the cost per iteration and therefore one factor of the required compu-

Model	#Param(M)	Iter.	FID↓
DiT-S/2 [35]			68.40
+ TREAD-1	33	400K	58.65
+ TREAD-2			54.79
DiT-B/2 [35]			43.47
+ TREAD-1 (random)	130	400K	36.80
+ TREAD-1			35.78
+ TREAD-2			28.80
DiT-XL/2 [35]			19.47
+ TREAD-1	675	400K	12.47
+ TREAD-2			10.63

Table 1. Performance comparison between the standard training method for diffusion models and our method using the same architectures each trained up to a maximum of 400k iterations. We demonstrate better performance across all model sizes.

Model	#Param(M)	Iter.	FID↓
RWKV [12]			59.84
+ TREAD-1	210	400K	53.79

Table 2. Result of Diffusion-RWKV_{+TREAD-1} with the RWKV[36] backbone to represent a broader application space.

tational budget. This is illustrated in Figure 4, where DiT, MaskDiT and MDT are used as baselines to compare absolute (FID vs. Iterations) and relative performance (FID vs. Training Hours) and the cost per iteration (it/s). TREAD performs favorably against all baselines across all presented ways that serve as measurement for convergence speed. With (it/s = 3.03) TREAD exhibits higher speed and therefore lower costs compared to MaskDiT (it/s = 2.98), the baseline DiT (it/s = 1.86) and MDT (it/s = 1.02) under identical settings. Next, we calculate the overall convergence speedup compared to a vanilla DiT. For this, we refer to the values in Table 3. Specifically we compare our DiT-XL/2_{+TREAD-2} at 400K steps (FID = 10.63) to DiT-XL/2 at 2352K steps (FID = 10.67) which results in a $5.88 \times$ speedup. Taking the cost per iteration into account as shown in Figure 4, we reach a convergence speedup of **9.55**. Taking the FID = 9.62 as a base, which is achieved by the vanilla DiT at 7M steps, we are able to provide a speedup factor of **25.39**. This speedup is demonstrated in Figure 1. While we reach comparable performance to MDT-XL/2, DiT-XL/2_{+TREAD-2} only requires nearly $1/10$ of the iterations. Additionally, we offer extrapolations of required training time, based on our measured iteration speed in Table 3.

5.3. Performance on other benchmark settings

We chose ImageNet512 in addition to our main results on ImageNet256 to showcase the scaling to larger token numbers.

Model	Iter.	FID ↓	Time [h]
MaskDiT-XL/2 [58]	400K	20.81	37.66
MDT-XL/2 [13]	400K	16.42	108.93
DiT-XL/2 [35]	400K	19.47	60.06
+ TREAD-2	400K	10.63	36.79
ADM [7]	1980K	10.94	–
MaskDiT-XL/2 [58]	2500K	10.06	235.40
MDT-XL/2 [13]	2500K	7.41	680.82
MDT-XL/2 [13]	6500K	6.23	1770.15
SD-DiT-XL/2 [59]	2400K	7.21	–
DiT-XL/2 [35]	7000K	9.62	1051.05
+ TREAD-2	700K	6.58	64.38

Table 3. Performance comparison between various DiT-based architectures that apply masking, vanilla DiT, and our routing training strategy. All models are based on the XL/2 type and are trained on ImageNet 256×256 with a batch size of 256 in the class-conditional setting, and sampling was done without classifier-free guidance.

Further, we transition to a text-to-image setting using the MSCOCO dataset. For both tasks we use the B/2 model size and evaluate the FID on 10,000 samples, without classifier-free guidance after 400K training iterations. We do not adapt our method in any way to the new tasks and utilize an identical setup to our main study on ImageNet256.

ImageNet 512			
Model	Iter.	FID ↓	FLOPS (G)
DiT	400K	62.8	21.81
+ TREAD-2	400K	40.9	13.65
MS-COCO			
DiT	400K	35.68	28.47
+ TREAD-2	400K	20.55	20.31

Table 4. Performance comparison of DiT-B/2 and DiT-B/2_{+TREAD-2} on the ImageNet 512×512 and MSCOCO datasets. FID scores indicate the quality of generated images, where lower values are better. The number of training iterations was set to 400K for all experiments and the number of FLOPS is calculated for a training pass that includes the application of routes. For both settings we achieve significantly better performance while being offering a more efficient training setup.

5.4. Ablation Study

We conduct multiple ablation studies to examine the effect that each component has on the performance of TREAD. All experiments are conducted using a DiT-B/2 model and evaluated using 50,000 samples except in Table 6 presented

results which use a DiT-S/2 and 10,000 samples for evaluation.

Selection Rate. In this experiment, we ablate the impact of the selection ratio on performance, which is shown in Table 5. We notice a significant boost in performance when employing a random selection rate of 0.25 (FID = 39.30) and 0.5 (FID = 35.78) outperforming the vanilla DiT-B/2 (FID = 43.47) on top of the significant reduction of cost per iteration. Interestingly, the medium selection rate of 0.5 resulted in better FID than 0.25. We attribute this behavior to the fact that the selection rate directly influences the number of tokens that first get withheld but, more importantly, get reintroduced into deeper layers of the network. Consequently, this means that the reintroduction of a larger portion of tokens can make up for lacking information in previous parts of the network. Further, we find the rate of 0.75 (FID = 72.30) to be too high, resulting in degraded performance compared to its vanilla counterpart. This indicates a optimal spot that maximizes the combination of performance and cost reduction between 0.5 and 0.75.

Model Type	Selection Rate	FID ↓
DiT-B/2+TREAD-1(random)	0.25	39.30
	0.50	35.78
	0.75	72.30

Table 5. Token selection ratios for the predefined routes using $\mathbf{r}_{0,8}$ on DiT-B/2. We notice a better performance with a moderate rate of 0.5 in comparison to the low 0.25 and high 0.75 rates. The gap between low and moderate rates especially underlines the usefulness of convergence that our proposed strategy provides.

Route Location. Next, we experiment with the locations inside of our model that we determine as the start and end of our token route \mathbf{r} . For this, iterate over the grid of possible combinations of route $\mathbf{r}_{i,j}$. The results of this are shown in Table 6. We find that the choice of i and j seems to be fairly arbitrary with the exception of $\mathbf{r}_{8,10}$, which resulted in the worst performance (FID = 232.53). We attribute this to the fact that the model does not have enough capacity after the tokens get reintroduced to process them appropriately. However, disregarding this exception, we notice that the specific variants of $\mathbf{r}_{i,j}$ do not have immense impacts on the overall performance of the model. This is also underlined by the near equal performance of DiT-B/2+TREAD-1 (FID = 35.78) and DiT-B/2+TREAD-1 (random) (FID = 36.80) as shown in Table 1. Therefore, we optimize for long routes to leverage the positive effects that routing has on the computational cost.

Multi-Route Loss. Applying multiple routes \mathbf{r} and therefore also multiple binary masks associated with each leads

Start(i) \ End(j)	0	2	4	6	8
2	103.40	-	-	-	-
4	97.02	93.21	-	-	-
6	95.17	94.98	94.11	-	-
8	96.27	102.64	97.69	108.29	-
10	118.10	101.39	103.41	103.49	232.53

Table 6. Comparisons of FID between different route configurations $\mathbf{r}_{i,j}$ on S/4 models trained on 400K iterations and evaluated using 10,000 samples. It is notable that all evaluations are numerically fairly close, with the distinction of $\mathbf{r}_{i,10}$ showing a substantially worse FID. We attribute this to the fact that the model lacks significant computational power to recover from the masking and utilize the introduced information.

Model	FID ↓
DiT-B/2	43.47
+ TREAD-2	28.80
w/o \mathbf{x}_t	37.65
w/o $D_\theta^{l_{j-1}}(\cdot, \cdot)$ w.r.t. $\mathbf{r}_{j,k}$	50.31
w/o Multi-Route Loss	44.54

Table 7. Ablation over the components in the linear combination $\gamma_{t,j-1}$ and the effect of the Multi-Route Loss on FID in a DiT-B/2+TREAD-2. We demonstrate that every presented component is vital to the performance of the model, with \mathbf{x}_t having the least impact on FID while still significantly falling behind DiT-B/2+TREAD-2. Not utilizing previously formed representations over the entire token set $D_\theta^{l_{j-1}}(\cdot, \cdot)$ deteriorates the performance significantly, and not incorporating all routes \mathbf{r} and their corresponding binary masks into the loss sees similar results.

to a shuffle between $\bar{\mathbf{v}}_m^1(\mathbf{x}_t)$ and $\bar{\mathbf{v}}_m^k(D_\theta^{l_{j-1}}(\cdot, \cdot))$ which renders the loss presented in Equation (10) insufficient. Therefore, we apply the in Equation (15) presented loss. In Table 7, the effect of leaving out this Multi-Route Loss is demonstrated by using two routes and only reflecting the effect of the first \mathbf{r} into the loss.

Linear Combination of Feature Maps. As mentioned in Section 4, all routes, except for the first, face the choice between incorporating \mathbf{x}_t or the last formed representation over all tokens $D_\theta^{l_{j-1}}(\cdot, \cdot)$ w.r.t. some route $\mathbf{r}_{i,j}$. This decision is circumvented by using a linear combination $\gamma_{t,j-1}$ of both with the advantages that the introduction of \mathbf{x}_t brings without disregarding already formed representations. In Table 7, it is demonstrated how leaving out one of these components can impact the performance respectively. As expected, the resulting DiT-B/2 models show deteriorated performance without $D_\theta^{l_{j-1}}(\cdot, \cdot)$ as this forces more task complexity into deeper layers due to missing intermediate representations. Not in-

cluding x_t still shows higher FID than DiT-B/2+TREAD-2 as well, underlining its importance.

6. Conclusion

In this work, we propose a diffusion training strategy, TREAD, that can be applied to any architecture without requiring extensions or adaptations. It offers increased performance and lower computational cost simultaneously by routing noisy tokens into deeper layers. Further, it offers great flexibility while retaining good robustness through arbitrary route locations. Overall, this results in convergence speedups on ImageNet-1K 256×256 by roughly one order of magnitude compared to the standard training of diffusion models. Our extensive experiments demonstrate that we achieve competitive benchmark results, even with limited computational resources.

Acknowledgement

This project has been supported by the German Federal Ministry for Economic Affairs and Climate Action within the project “NXT GEN AI METHODS – Generative Methoden für Perzeption, Prädiktion und Planung”, the bidt project KLIMA-MEMES, Bayer AG, and the German Research Foundation (DFG) project 421703927. The authors gratefully acknowledge the Gauss Center for Supercomputing for providing compute through the NIC on JUWELS at JSC and the HPC resources supplied by the Erlangen National High Performance Computing Center (NHR@FAU funded by DFG).

References

- [1] Benedikt Alkin, Maximilian Beck, Korbinian Pöppel, Sepp Hochreiter, and Johannes Brandstetter. Vision-1stm: xlstm as generic vision backbone, 2024. 13
- [2] Mahmoud Assran, Quentin Duval, Ishan Misra, Piotr Bojanowski, Pascal Vincent, Michael Rabbat, Yann LeCun, and Nicolas Ballas. Self-supervised learning from images with a joint-embedding predictive architecture, 2023. 2
- [3] Andreas Blattmann, Robin Rombach, Huan Ling, Tim Dockhorn, Seung Wook Kim, Sanja Fidler, and Karsten Kreis. Align your latents: High-resolution video synthesis with latent diffusion models. In *CVPR*, 2023. 1
- [4] Pascal Chang, Jingwei Tang, Markus Gross, and Vinicius C Azevedo. How i warped your noise: a temporally-correlated noise prior for diffusion models. In *The Twelfth International Conference on Learning Representations*, 2024. 4
- [5] Junsong Chen, Jincheng Yu, Chongjian Ge, Lewei Yao, Enze Xie, Yue Wu, Zhongdao Wang, James Kwok, Ping Luo, Huchuan Lu, and Zhenguo Li. Pixart- α : Fast training of diffusion transformer for photorealistic text-to-image synthesis. *ICLR*, 2024. 2
- [6] Jacob Devlin, Ming-Wei Chang, Kenton Lee, and Kristina Toutanova. BERT: Pre-training of deep bidirectional transformers for language understanding. In *Proceedings of the 2019 Conference of the North American Chapter of the Association for Computational Linguistics: Human Language Technologies, Volume 1 (Long and Short Papers)*, pages 4171–4186, Minneapolis, Minnesota, 2019. Association for Computational Linguistics. 2
- [7] Prafulla Dhariwal and Alexander Nichol. Diffusion models beat gans on image synthesis. *NeurIPS*, 2021. 2, 6, 7, 12, 14
- [8] Patrick Esser, Sumith Kulal, Andreas Blattmann, Rahim Entezari, Jonas Müller, Harry Saini, Yam Levi, Dominik Lorenz, Axel Sauer, Frederic Boesel, Dustin Podell, Tim Dockhorn, Zion English, Kyle Lacey, Alex Goodwin, Yannik Marek, and Robin Rombach. Scaling rectified flow transformers for high-resolution image synthesis. *ICML*, 2024. 2
- [9] Mohsen Fayyaz, Sorous Abbasi Kouhpayegani, Farnoush Rezaei Jafari, Eric Sommerlade, Hamid Reza Vaezi Joze, Hamed Pirsiavash, and Juergen Gall. Adaptive token sampling for efficient vision transformers. *European Conference on Computer Vision (ECCV)*, 2022. 3
- [10] Zhengcong Fei, Mingyuan Fan, Changqian Yu, and Junshi Huang. Scalable diffusion models with state space backbone, 2024. 2
- [11] Zhengcong Fei, Mingyuan Fan, Changqian Yu, Debang Li, and Junshi Huang. Scaling diffusion transformers to 16 billion parameters. *arXiv preprint*, 2024. 2
- [12] Zhengcong Fei, Mingyuan Fan, Changqian Yu, Debang Li, and Junshi Huang. Diffusion-rwkv: Scaling rwkv-like architectures for diffusion models. *arXiv preprint arXiv:2404.04478*, 2024. 2, 5, 7, 13
- [13] Shanghua Gao, Pan Zhou, Ming-Ming Cheng, and Shuicheng Yan. Masked diffusion transformer is a strong image synthesizer. In *Proceedings of the IEEE/CVF International Conference on Computer Vision (ICCV)*, pages 23164–23173, 2023. 1, 2, 6, 7, 12, 14
- [14] Ian Goodfellow, Jean Pouget-Abadie, Mehdi Mirza, Bing Xu, David Warde-Farley, Sherjil Ozair, Aaron Courville, and Yoshua Bengio. Generative adversarial networks. *Communications of the ACM*, 63(11):139–144, 2020. 1
- [15] Albert Gu and Tri Dao. Mamba: Linear-time sequence modeling with selective state spaces. *COLM*, 2024. 13
- [16] Agrim Gupta, Stephen Tian, Yunzhi Zhang, Jiajun Wu, Roberto Martín-Martín, and Li Fei-Fei. Maskvit: Masked visual pre-training for video prediction, 2022. 2
- [17] Kaiming He, Xinlei Chen, Saining Xie, Yanghao Li, Piotr Dollár, and Ross Girshick. Masked autoencoders are scalable vision learners. In *CVPR*, 2022. 2, 3
- [18] Shwai He, Guoheng Sun, Zheyu Shen, and Ang Li. What matters in transformers? not all attention is needed. *CoRR*, abs/2406.15786, 2024. 2, 4
- [19] Martin Heusel, Hubert Ramsauer, Thomas Unterthiner, Bernhard Nessler, and Sepp Hochreiter. Gans trained by a two time-scale update rule converge to a local nash equilibrium. In *NeurIPS*, 2017. 6, 14
- [20] Jonathan Ho, Ajay Jain, and Pieter Abbeel. Denoising diffusion probabilistic models. In *NeurIPS*, 2020. 1, 2
- [21] Vincent Tao Hu, David W Zhang, Yuki M Asano, Gertjan J Burghouts, and Cees GM Snoek. Self-guided diffusion models. In *Proceedings of the IEEE/CVF Conference on Com-*

- puter Vision and Pattern Recognition*, pages 18413–18422, 2023. 1
- [22] Vincent Tao Hu, Stefan Andreas Baumann, Ming Gui, Olga Grebenkova, Pingchuan Ma, Johannes Fischer, and Björn Ommer. Zigma: A dit-style zigzag mamba diffusion model. In *ECCV*, 2024. 1, 2, 3, 13
- [23] Robert A. Jacobs, Michael I. Jordan, Steven J. Nowlan, and Geoffrey E. Hinton. Adaptive Mixtures of Local Experts. *Neural Computation*, 3(1):79–87, 1991. 2
- [24] Tero Karras, Miika Aittala, Timo Aila, and Samuli Laine. Elucidating the design space of diffusion-based generative models. In *NeurIPS*, 2022. 3, 12, 16, 17
- [25] Tuomas Kynkäänniemi, Tero Karras, Samuli Laine, Jaakko Lehtinen, and Timo Aila. Improved precision and recall metric for assessing generative models. *Advances in neural information processing systems*, 32, 2019. 14
- [26] Zhengyang Liang, Hao He, Ceyuan Yang, and Bo Dai. Scaling laws for diffusion transformers, 2024. 1
- [27] Yaron Lipman, Ricky TQ Chen, Heli Ben-Hamu, Maximilian Nickel, and Matt Le. Flow matching for generative modeling. In *ICLR*, 2023. 2
- [28] Nanye Ma, Mark Goldstein, Michael S. Albergo, Nicholas M. Boffi, Eric Vanden-Eijnden, and Saining Xie. Sit: Exploring flow and diffusion-based generative models with scalable interpolant transformers, 2024. 14
- [29] Xinyin Ma, Gongfan Fang, and Xinchao Wang. Deepcache: Accelerating diffusion models for free, 2023. 2, 4
- [30] Xinyin Ma, Gongfan Fang, Michael Bi Mi, and Xinchao Wang. Learning-to-cache: Accelerating diffusion transformer via layer caching, 2024. 2, 4
- [31] Song Mei and Yuchen Wu. Deep networks as denoising algorithms: Sample-efficient learning of diffusion models in high-dimensional graphical models, 2023. 1
- [32] Lingchen Meng, Hengduo Li, Bor-Chun Chen, Shiyi Lan, Zuxuan Wu, Yu-Gang Jiang, and Ser-Nam Lim. Advait: Adaptive vision transformers for efficient image recognition. In *Proceedings of the IEEE/CVF Conference on Computer Vision and Pattern Recognition (CVPR)*, pages 12309–12318, 2022. 2, 3
- [33] Charlie Nash, Jacob Menick, Sander Dieleman, and Peter W Battaglia. Generating images with sparse representations. *arXiv preprint arXiv:2103.03841*, 2021. 14
- [34] Byeongjun Park, Hyojun Go, Jin-Young Kim, Sangmin Woo, Seokil Ham, and Changick Kim. Switch diffusion transformer: Synergizing denoising tasks with sparse mixture-of-experts, 2024. 2
- [35] William Peebles and Saining Xie. Scalable diffusion models with transformers. *ICCV*, 2023. 1, 2, 5, 6, 7, 12, 14
- [36] Bo Peng, Eric Alcaide, Quentin Anthony, Alon Albalak, Samuel Arcadinho, Stella Biderman, Huanqi Cao, Xin Cheng, Michael Chung, Matteo Grella, et al. Rwkv: Reinventing rnns for the transformer era. *EMNLP Finding*, 2023. 3, 7
- [37] Maciej Pióro, Kamil Ciebiera, Krystian Król, Jan Ludziejewski, Michał Krutul, Jakub Krajewski, Szymon Antoniak, Piotr Miłoś, Marek Cygan, and Sebastian Jaszczur. Moe-mamba: Efficient selective state space models with mixture of experts, 2024. 2
- [38] Ben Poole, Ajay Jain, Jonathan T. Barron, and Ben Mildenhall. Dreamfusion: Text-to-3d using 2d diffusion. In *The Eleventh International Conference on Learning Representations*, 2023. 1
- [39] Yongming Rao, Wenliang Zhao, Benlin Liu, Jiwen Lu, Jie Zhou, and Cho-Jui Hsieh. Dynamicvit: Efficient vision transformers with dynamic token sparsification. In *Advances in Neural Information Processing Systems*, pages 13937–13949. Curran Associates, Inc., 2021. 3
- [40] David Raposo, Sam Ritter, Blake Richards, Timothy Lillicrap, Peter Conway Humphreys, and Adam Santoro. Mixture-of-depths: Dynamically allocating compute in transformer-based language models. *arXiv preprint arXiv:2404.02258*, 2024. 2, 4, 13
- [41] Robin Rombach, Andreas Blattmann, Dominik Lorenz, Patrick Esser, and Björn Ommer. High-resolution image synthesis with latent diffusion models. In *CVPR*, 2022. 1, 2, 5, 14
- [42] Olaf Ronneberger, Philipp Fischer, and Thomas Brox. U-net: Convolutional networks for biomedical image segmentation. 2015. 2
- [43] Dvir Samuel, Barak Meiri, Haggai Maron, Yoad Tewel, Nir Darshan, Shai Avidan, Gal Chechik, and Rami Ben-Ari. Lightning-fast image inversion and editing for text-to-image diffusion models, 2024. 4
- [44] Noam Shazeer, Azalia Mirhoseini, Krzysztof Maziarz, Andy Davis, Quoc Le, Geoffrey Hinton, and Jeff Dean. Outrageously large neural networks: The sparsely-gated mixture-of-experts layer, 2017. 2
- [45] Jascha Sohl-Dickstein, Eric Weiss, Niru Maheswaranathan, and Surya Ganguli. Deep unsupervised learning using nonequilibrium thermodynamics. In *ICML*, 2015. 1
- [46] Yang Song and Stefano Ermon. Generative modeling by estimating gradients of the data distribution. *Advances in neural information processing systems*, 32, 2019. 2
- [47] Yang Song and Stefano Ermon. Improved techniques for training score-based generative models. *Advances in neural information processing systems*, 33:12438–12448, 2020. 2
- [48] Yang Song, Jascha Sohl-Dickstein, Diederik P Kingma, Abhishek Kumar, Stefano Ermon, and Ben Poole. Score-based generative modeling through stochastic differential equations. In *ICLR*, 2021. 3
- [49] Haotian Sun, Tao Lei, Bowen Zhang, Yanghao Li, Haoshuo Huang, Ruoming Pang, Bo Dai, and Nan Du. Ec-dit: Scaling diffusion transformers with adaptive expert-choice routing, 2024. 2
- [50] Fenghe Tang, Bingkun Nian, Yingtai Li, Jie Yang, Liu Wei, and S. Kevin Zhou. Mambamim: Pre-training mamba with state space token-interpolation, 2024. 2
- [51] Yao Teng, Yue Wu, Han Shi, Xuefei Ning, Guohao Dai, Yu Wang, Zhenguo Li, and Xihui Liu. Dim: Diffusion mamba for efficient high-resolution image synthesis, 2024. 2
- [52] Alexander Tong, Kilian FATRAS, Nikolay Malkin, Guillaume Huguet, Yanlei Zhang, Jarrid Rector-Brooks, Guy Wolf, and Yoshua Bengio. Improving and generalizing flow-based generative models with minibatch optimal transport. *Transactions on Machine Learning Research*, 2024. Expert Certification. 2

- [53] Ashish Vaswani, Noam Shazeer, Niki Parmar, Jakob Uszkoreit, Llion Jones, Aidan N Gomez, Łukasz Kaiser, and Illia Polosukhin. Attention is all you need. *NeurIPS*, 2017. [1](#)
- [54] Hongjie Wang, Difan Liu, Yan Kang, Yijun Li, Zhe Lin, Niraj K. Jha, and Yuchen Liu. Attention-driven training-free efficiency enhancement of diffusion models, 2024. [2](#), [3](#)
- [55] Sihyun Yu, Sangkyung Kwak, Huiwon Jang, Jongheon Jeong, Jonathan Huang, Jinwoo Shin, and Saining Xie. Representation alignment for generation: Training diffusion transformers is easier than you think. *arXiv preprint arXiv:2410.06940*, 2024. [1](#), [6](#)
- [56] Zheng Zhan, Zhenglun Kong, Yifan Gong, Yushu Wu, Zichong Meng, Hangyu Zheng, Xuan Shen, Stratis Ioannidis, Wei Niu, Pu Zhao, and Yanzhi Wang. Exploring token pruning in vision state space models. *NeurIPS*, 2024. [2](#)
- [57] Hongyi Zhang, Moustapha Cisse, Yann N Dauphin, and David Lopez-Paz. mixup: Beyond empirical risk minimization. In *ICLR*, 2017. [2](#)
- [58] Hongkai Zheng, Weili Nie, Arash Vahdat, and Anima Anandkumar. Fast training of diffusion models with masked transformers. *TMLR*, 2024. [1](#), [2](#), [3](#), [6](#), [7](#), [12](#), [14](#), [15](#)
- [59] Rui Zhu, Yingwei Pan, Yehao Li, Ting Yao, Zhenglong Sun, Tao Mei, and Chang Wen Chen. Sd-dit: Unleashing the power of self-supervised discrimination in diffusion transformer. In *CVPR*, pages 8435–8445, 2024. [1](#), [3](#), [7](#), [12](#), [14](#), [15](#)

A. Implementation Details

A.1. Experimental Configuration

In contrast to DiT [35] and MDT [13], which leverage the ADM framework [7], our experimental approach is grounded in the formulation of EDM [24]. Specifically, we implement EDM’s preconditioning through a σ -dependent skip connection, utilizing the standard parameter settings.

This approach eliminates the necessity to train ADM’s noise covariance parameterization, as required by DiT. For the inference phase, we adopt the default temporal schedule defined by:

$$t_{i < N} = \left(t_{\max}^{\frac{1}{\rho}} + \frac{i}{N-1} \left(t_{\min}^{\frac{1}{\rho}} - t_{\max}^{\frac{1}{\rho}} \right) \right)^{\rho}, \quad (16)$$

where the parameters are set to $N = 40$, $\rho = 7$, $t_{\max} = 80$, and $t_{\min} = 0.002$. Furthermore, we employ Heun’s method as the ODE solver for the sampling process. This choice has been shown to achieve FID scores comparable to those obtained with 250 DDPM steps while significantly reducing the number of required steps [24, 58].

The noise distribution adheres to the EDM configuration, defined by:

$$\ln(p_{\sigma}) \sim \mathcal{N}(P_{\text{mean}}, P_{\text{std}}), \quad (17)$$

with $P_{\text{mean}} = -1.2$ and $P_{\text{std}} = 1.2$. For detailed information, refer to the EDM paper [24].

A.2. Network Details

Specific Routes In Table 8, we specify the exact routes \mathbf{r} used for each model type. We ensure that the first route always begins at $D_{\theta}^{i_0}$ to maximize the potential length that the route \mathbf{r} spans. Given that the design space of TREADis inherently constrained by the number of layers, we choose different route endings for various model sizes. In the multi-route setting, we leverage the insights from Table 6 and introduce a few computational blocks between two distinct routes.

Model	# of Routes	Route
DiT-S	1	$\mathbf{r}_{0,8}$
DiT-S	2	$\mathbf{r}_{0,4}, \mathbf{r}_{6,9}$
DiT-B	1	$\mathbf{r}_{0,8}$
DiT-B (random)	1	$\mathbf{r}_{0,g}$
DiT-B	2	$\mathbf{r}_{0,4}, \mathbf{r}_{6,9}$
DiT-XL	1	$\mathbf{r}_{0,21}$
DiT-XL	2	$\mathbf{r}_{0,10}, \mathbf{r}_{13,21}$
RWKV	1	$\mathbf{r}_{0,8}$

Table 8. The exact routes $\mathbf{r}_{i,j}$ applied to each model size. DiT-B (random) applies a random route for each forward pass with $g \in [2, 8]$.

Model	# of Parameters (Millions)
DiT	675
DiT+TREAD	675
MaskDiT	730
SD-DiT	740

Table 9. Comparison of the number of network parameters. MaskDiT and SD-DiT add a substantial number of parameters, approximately 10% of those in XL-sized DiT models. This additional parameter count is fixed across different model sizes [58, 59], which can slow down smaller models since the relative size of the added decoder components increases.

Parameter Comparison As previously discussed, our method does not require any modifications to the architecture itself, whereas other methods incorporate a predefined decoder head on top of the standard DiT structure. This introduces computational overhead that is particularly noticeable in smaller models. Since our method does not need these additional parameters, we reduce the computational cost associated with the decoder head. This is demonstrated in Table 9.

Diffusion-RWKV Setting Due to the nature of RWKV and other state-space models (SSMs) [1, 15, 22], a row selection strategy is applied instead of a random selection. Additionally, we adhere to the DiT configuration in the RWKV setting. Nevertheless, we are able to improve upon our own Diffusion-RWKV [12] baseline using TREAD. The poor performance of our RWKV baseline can be attributed to the number of layers; our model consists of only 12 layers, whereas [12] recommends using 25 or even 49 layers.

Pruning, Masking & Routing In Figure 5, we provide an overview of pruning, masking, and routing. While pruning can be seen as a subcategory of masking where tokens are removed based on importance or a learned heuristic, routing does not remove tokens but merely withholds them from computational blocks.

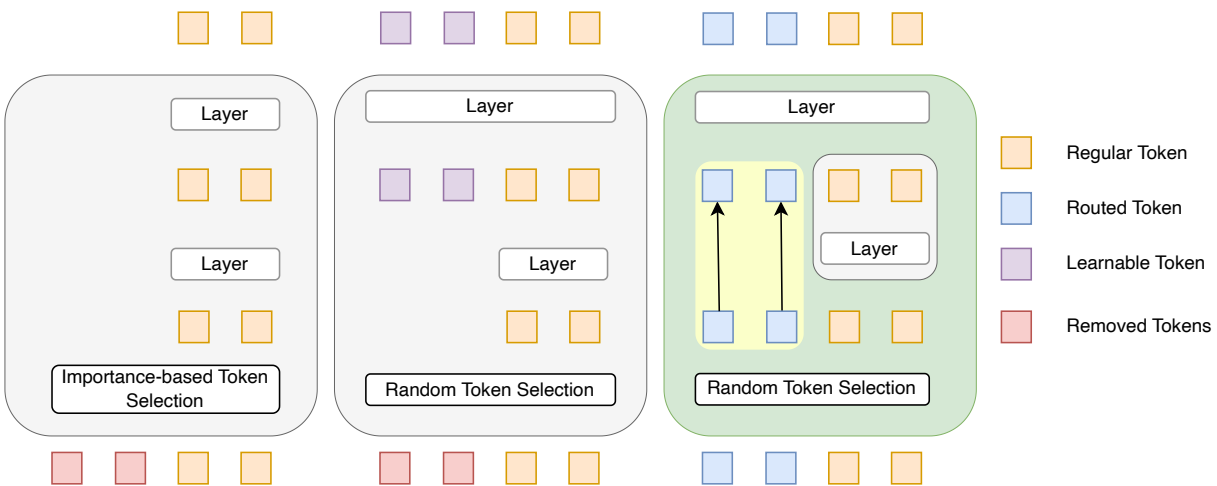


Figure 5. Comparison of three techniques for reducing the number of processed tokens: token pruning (left), masking (middle), and routing (right). Token pruning involves decreasing the token count by eliminating redundant tokens and retaining only the most important ones. This method can be considered a subset of masking, which broadly encompasses techniques that reduce the number of tokens by randomly selecting and discarding them. In contrast, routing aims to achieve the primary goal of reducing computational resource usage through fundamentally different mechanisms. Routing can be implemented either randomly or via a learned function, as demonstrated by Raposo et al. [40]. Importantly, routing does not result in permanent information loss; instead, the omitted tokens are merely withheld from specific computational blocks, ensuring that information remains accessible within the model.

A.3. Pseudocode for a forward pass with a single route

Algorithm 1 Forward Pass with Routes in TREAD

Require:

```

1: Input tokens  $\mathbf{x}$ 
2: Timestep  $t$ 
3: Class label  $y$ 
4: Route strategy route_strat (Vector indicating route actions at each layer)
5: Initialize:
6:    $\mathbf{x} \leftarrow \text{Embed}(\mathbf{x})$ 
7:    $\mathbf{c} \leftarrow \text{Condition}(t, y)$ 
8:    $\mathbf{x}_{\text{orig}} \leftarrow \mathbf{x}$ 
9: for  $i = 1$  to  $B$  do
10:  action  $\leftarrow$  route_strat[ $i$ ]
11:  if action = 1 then ▷ Route starts at layer  $i$ 
12:     $\mathbf{x}_{\text{skip}} \leftarrow \mathbf{x}$ 
13:     $\mathbf{x} \leftarrow \text{ApplySelection}(\mathbf{x}, \text{route})$ 
14:  end if
15:   $\mathbf{x} \leftarrow \text{ProcessLayer}(\mathbf{x}, \mathbf{c})$ 
16:  if action = -1 then ▷ Route ends at layer  $i$ 
17:     $\mathbf{x}_{\text{reintro}} \leftarrow \mathbf{x}_{\text{orig}} + \mathbf{x}_{\text{skip}}$ 
18:     $\mathbf{x} \leftarrow \text{ReintroduceTokens}(\mathbf{x}, \mathbf{x}_{\text{reintro}})$ 
19:  end if
20: end for
21: return  $\mathbf{x}$ 

```

B. More Extensive Comparison

In this work, we consider FID [19] to still be the main metric of comparison between generative methods for class-conditional image synthesis even though other metrics exist [25, 33] exist. In Table 10, we provide a more extensive evaluation against both our baselines and as well as an additional set of methods that are often referred to.

Method	FID↓	sFID↓	IS↑	Prec.↑	Rec.↑
<i>Pixel-based diffusion methods</i>					
ADM [7]	10.94	6.02	100.98	0.69	0.63
ADM-U [7]	7.49	5.13	127.49	0.72	0.63
<i>Latent-based diffusion methods</i>					
U-Net-based architectures					
LDM-8 [41]	15.51	-	79.03	0.65	0.63
LDM-4 [41]	10.56	-	209.52	0.84	0.35
Transformer-based architectures					
DiT-XL/2 [35]	9.62	6.85	121.50	0.67	0.67
DiT-XL/2+TREAD-2 (ours)	6.58	6.32	136.82	0.76	0.56
SiT-XL/2 [28]	8.61	6.32	131.65	0.68	0.67
SD-DiT-XL/2 [59]	7.21	5.17	144.68	0.72	0.61
MDT-XL/2 [13]	6.23	5.23	143.02	0.71	0.65
MaskDiT-XL/2 [58]	5.69	10.34	177.99	0.74	0.60

Table 10. Absolute performance comparison of various diffusion-based methods categorized by type and architectures without considering the computational cost (iterations and batch size). FID [19] and sFID [33] measure fidelity, IS represents Inception Score, and Precision/Recall [25]. For both FID and sFID, the lower, the better, while for IS and Precision/Recall, higher is better.

Classifier-free Guidance We apply Classifier-free Guidance (CFG) to our DiT-XL/2+TREAD-2. We reach an FID of 3.40 after only 700K training iterations with routing, which is competitive with other efficiency-based methods [58, 59]. We further show the FID without CFG (CFG=1.0) and with CFG (CFG=1.5) during the progress of training in Figure 6

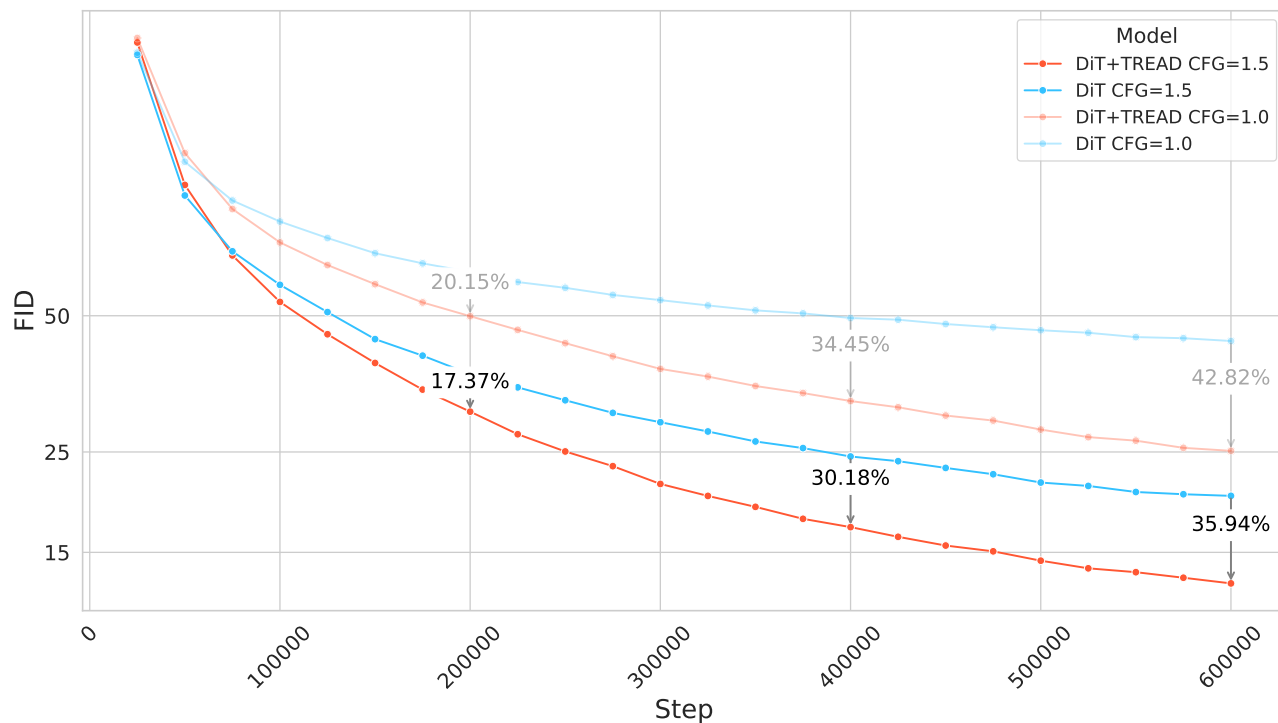


Figure 6. Comparison between FID (CFG=1.0) against FID (CFG=1.5) across training iterations of a DiT-B/2 and DiT-B/2+TREAD-2 model using 10K samples. We show that our method outperforms our standard baseline using the no classifier-free guidance (CFG=1.0) as well as the standard scale (CFG=1.5) for ImageNet256.

C. Examples



Figure 7. Selected samples produced with DiT-XL/2₊TREAD-2 (+CFG). We use 40 deterministic EDM [24] steps.

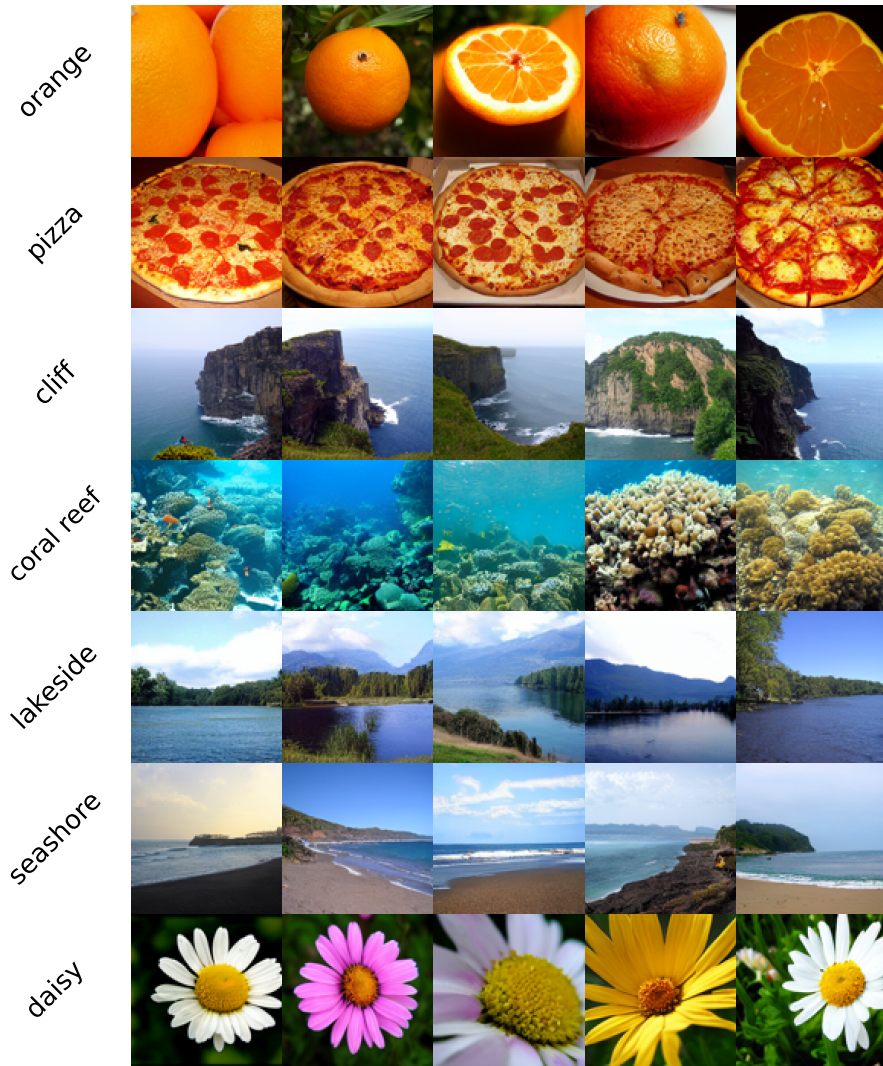


Figure 8. Selected samples produced with DiT-XL/2₊TREAD-2 (+CFG). We use 40 deterministic EDM [24] steps.